

Simulating the morphology and mechanical properties of filled diblock copolymers

Gavin A. Buxton and Anna C. Balazs

Department of Chemical and Petroleum Engineering, University of Pittsburgh, Pittsburgh, Pennsylvania 15261

(Received 4 November 2002; published 14 March 2003)

We couple a morphological study of a mixture of diblock copolymers and spherical nanoparticles with a micromechanical simulation to determine how the spatial distribution of the particles affects the mechanical behavior of the composite. The morphological studies are conducted through a hybrid technique, which combines a Cahn-Hilliard (CH) theory for the diblocks and a Brownian dynamics (BD) for the particles. Through these “CH-BD” calculations, we obtain the late-stage morphology of the diblock-particle mixtures. The output of this CH-BD model serves as the input to the lattice spring model (LSM), which consists of a three-dimensional network of springs. In particular, the location of the different phases is mapped onto the LSM lattice and the appropriate force constants are assigned to the LSM bonds. A stress is applied to the LSM lattice, and we calculate the local strain fields and overall elastic response of the material. We find that the confinement of nanoparticles within a given domain of a bicontinuous diblock mesophase causes the particles to percolate and form essentially a rigid backbone throughout the material. This continuous distribution of fillers significantly increases the reinforcement efficiency of the nanoparticles and dramatically increases the Young’s modulus of the material. By integrating the morphological and mechanical models, we can isolate how modifications in physical characteristics of the particles and diblocks affect both the structure of the mixture and the macroscopic behavior of the composite. Thus, we can establish how choices made in the components affect the ultimate performance of the material.

DOI: 10.1103/PhysRevE.67.031802

PACS number(s): 62.20.Dc, 62.25.+g, 64.75.+g, 66.30.Jt

I. INTRODUCTION

The blending of nanoparticles and polymers provides a means of creating hybrid materials that integrate the desirable features of each of the constituents. For example, the particles impart stiffness and the polymers prevent the material from being brittle. If the nanoparticles are metals or semiconductors, the composite can exhibit the unique electrical, optical, or magnetic properties of the inorganics and the flexibility and processibility of the polymers. Recently, there has been considerable interest in blending nanoparticles and diblock copolymers [1–17] to create materials for flexible batteries [1], photonic band gap devices [6] and nanoelectrode arrays [13,14]. One of the challenges in designing such complex materials is predicting the macroscopic behavior of the composite based upon such constituent characteristics as the diblock architecture and the nanoparticle surface chemistry. By addressing this challenge, researchers could ultimately understand how choices made in the initial design stage affect the final materials’ performance and facilitate the efficient fabrication of composites with the desired properties.

Here, we seek to tackle this issue by integrating two different computational approaches and thereby relate the polymer architecture, the wetting interactions between the polymer and particles, the structure of the mixture, and the mechanical behavior of the resulting material. In particular, we use a hybrid method [18–23] that combines a Cahn-Hilliard (CH) model for the diblocks and a Brownian dynamics (BD) simulation for the particles in order to determine the structural evolution of the particle-filled copolymer melt. As we detail further below, the approach allows us to specify the architecture of the chains and the nature of the polymer-

particle interactions. In this paper, we will refer to this hybrid method as the CH-BD model.

The output of the CH-BD simulation then serves as the input to the lattice spring model (LSM), a micromechanical model that captures the elastic properties and mechanical response of the composite. By combining the CH-BD and LSM models, we can determine how the structural evolution, or the history of the material, affects the mechanical response [24]. Furthermore, we do not have to make *ad hoc* assumptions about the distribution of particles in the system; this distribution evolves naturally from the self-assembling interactions between the different components. Through the LSM, we can carry out three-dimensional simulations that include as many as 1564 particles. In particular, the studies reported here represent the first 3D studies on the mechanical properties of such extensive filled copolymer systems. The results allow us to determine how changes in the nature of the components influence the macroscopic properties of the composite.

One reason for focusing on mixtures of diblocks and nanoparticles is that the self-assembly of the diblocks can be exploited to direct the distribution of the nanoparticles within the mixture [8,25–27] and thus, achieve a degree of control over the morphology of the system. For example, if the particles are preferentially wetted by the *A* blocks of a system of *AB* diblocks, the particles will localize within the *A* domains of the microphase separated melt. In recent computational studies that involve the hybrid CH-BD model, Ginzburg *et al.* [23] showed that in the presence of the *AB* diblocks, these *A*-like particles in fact form a percolated network at a significantly lower volume fraction (essentially half) than would be required in a homogeneous material (i.e., homopolymer melt). In this study, one of our aims is to deter-

mine how these percolating networks act to reinforce the copolymer matrix.

The two main numerical techniques that can be used to investigate the reinforcing properties of the filler particles are the finite element method (FEM) and the LSM. The FEM, a discretized continuum model, is the dominant technique employed in micromechanical modeling. The FEM employs preprocessed mesh generation, which enables the model to fully capture the spatial discontinuities of highly inhomogeneous materials. The FEM techniques also allow complex, nonlinear tensile relationships to be incorporated into the analysis. In three dimensions, the FEM micromechanical simulations generally employ a unit-cell methodology or an axisymmetric approach; these models possess translational and reflective symmetry, respectively. Utilizing both unit-cell and axisymmetric systems, Christman *et al.* [28] and Llorca *et al.* [29] investigated SiC reinforced aluminum composites. Hom and McMeeking [30] employed a unit-cell simulation to study a cubic array of rigid spheres in an elastic-perfect plastic matrix. In order to investigate clustering effects, the particles may be displaced towards axisymmetric boundaries, although this assumes an infinite array of clustering effects [29,31]. A regular distribution of three clustered particles in an infinite system was modeled using an axisymmetric system by Thomson *et al.* [32]. A repeated pattern of particles allowed clustering effects to be considered, while particle decohesion was accounted for through the use of a traction-separation relation similar to Needleman [33]. Simulations addressing significantly larger collections of particles were performed by Gusev *et al.* [34], in which a periodic elastic system, containing up to 64 spherical particles, was used to calculate the overall elastic constants. Recently, a similar multiparticle system has been considered by Böhm [35], in which systems containing 20 particles were deformed. The number of particles that can be simulated is limited by the computational expense of the FEM, and a more computationally efficient technique is required to simulate larger system sizes.

The LSMs of elasticity consist of a network of interconnecting springs, the properties of which can be varied to tailor the response of the system and to ensure that the model conforms to elasticity theory. One variety of the LSM is the Born LSM, which is a macroscopic equivalent of the Born-Huang model for microscopic elasticity [36]. The extension of a spring is energetically penalized by way of a central force constant, while a lack of rotational freedom is imposed upon the springs through the introduction of a noncentral force constant [37,38]. Rotation of this system from the networks' original orientation results in a restoring force, although the configuration is otherwise unchanged. This lack of rotational invariance does not have a significant effect for small displacements [37], for which this model can be shown to be equivalent to the mathematical theory of an isotropic elastic continuum [39]. More complicated rotationally invariant three-body interactions have been considered [40], although the additional computational expense is unwarranted in systems where rotations are assumed to be small.

The majority of the LSM particulate simulations have been the two-dimensional investigations of circular inclu-

sions [41–45]. Recently, three-dimensional simulations have included a spherical particle in the presence of plasticity [39], while we have applied a three-dimensional multi-inclusion Born LSM to the numerical investigation of viscoelastic polymers reinforced with either platelets, rods, or spheres [46]. These studies reveal that the LSM is becoming an increasingly valuable technique in the numerical simulation of micromechanics. As we show in the studies described below, when the LSM is coupled with a computational model that reveals the morphology of complex mixtures, the integrated approach can be used to establish structure-property relationships for a broad class of materials.

It should be noted, however, that the application of continuum mechanics to systems on the nanoscale might be extending the traditional applicability of the LSM, since the mechanical behavior in nanocomposites is dictated by more discrete phenomena. That said, the potential wealth of qualitative information that can be obtained concerning the deformation of complex morphologies associated with nanocomposites warrants the application of such techniques.

This paper is organized as follows: in Sec. II, a description of the simulation techniques for modeling the structural evolution of diblock-particle mixtures and the micromechanics of solid polymeric composites is given. In Sec. III, we investigate the effects of varying the diblock copolymer architecture and particle volume fraction on the morphological and mechanical behavior. The effects of size and polydispersity in the particle system are also investigated. In Sec. IV, a summary of results is provided and conclusions are drawn.

II. MODEL

A. Determining the morphology of diblock-particle mixtures

The system consists of an AB diblock copolymer melt and mobile nanoparticles. We simulate the behavior of this mixture on a three-dimensional cubic lattice, which is 64^3 sites in size and has periodic boundary conditions in all three directions. The copolymer melt is characterized by the scalar order parameter Ψ which describes the local concentration difference between the A and B components. Note that $\Psi = -1$ (1) corresponds to the equilibrium order parameter for A -rich (B -rich) phase. In this version of the model, the particles in the system are “soft” or penetrable, since we neglect excluded volume interactions between the particles and the fluid. (Excluded volume interactions can be explicitly included in the model [23]; for corresponding systems, both the “hard” and “soft” fillers yield similar results for the particle distributions.) The particles have an affinity for the A block. This affinity is introduced via a polymer-particle coupling term in the free energy (as described below). Thus, the microphase separation of the diblocks can affect the spatial distribution of the particles and the particles can influence the size and morphology of the polymer domains.

The CH equation [47,48] describes the phase separation of a binary mixture by spinodal decomposition, in the absence of hydrodynamics. The dynamics of microphase segregation for a diblock copolymer melt is described by the traditional CH equation with the addition of the term $-\Gamma(\Psi - f)$ [49], where Γ determines the thickness of the

domain structure and f describes the asymmetry of the diblock. The case of $f=0$ describes a 50:50 symmetric diblock. The kinetic equation for the order parameter for this system is

$$\frac{\partial \Psi}{\partial t} = M \nabla^2 \frac{\delta F}{\delta \Psi} - \Gamma(\Psi - f) + \xi, \quad (1)$$

where M is the kinetic coefficient (mobility) of the order parameter field, and ξ is the noise field (which is presently set to zero). F is the local energy term and is given by $F = F_d + F_{cpl}$. In the current study, F_d is given by

$$F_d = \int -A \ln[\cos(\Psi)] + \frac{1}{2} \Psi^2 + \frac{D}{2} (\nabla \Psi)^2 \partial r, \quad (2)$$

where A and D are material specific parameters and the integration is over the volume of the system.

The nanoparticles are introduced through the coupling free energy, F_{cpl} . This free energy describes the interaction between the soft particles and the polymer, and ensures that the forces on the particle due to the presence of the polymer induce equal and opposite forces within the polymer. The coupling free energy is of the form

$$F_{cpl} = \zeta \int \sum_i U(r - x_i) [\Psi(r) - \Psi_s]^2 \partial r, \quad (3)$$

where ζ is a material constant, x_i is the position of the i^{th} particle, and Ψ_s is the desired value of the order parameter at the particle surface. To model the fact that the particles have an affinity for the A phase, we set $\Psi_s = -1$. The potential $U(\cdot)$ is nonlinear, and is given by

$$U(r - x_i) = \exp\left(-\frac{r - x_i - R}{r_0}\right) \quad \forall (r - x_i) > R, \quad (4)$$

$$U(r - x_i) = 1 \quad \forall (r - x_i) < R.$$

The parameter r_0 sets the range of the interaction and R is the radius of the particle.

The motion of the particles is dictated by the Langevin equation

$$\frac{\partial x_i}{\partial t} = -M_p \frac{\partial F}{\partial x_i} + \eta, \quad (5)$$

where M_p is the particle mobility and η is a Gaussian white noise term. It should be noted, however, that particles are prohibited from overlapping (i.e., if a particles' new position causes it to overlap with another particle, the move is rejected). In this sense, a hard core interaction between the particles is imposed. Through the coupled Eqs. (1) and (5), the ordering dynamics of the diblock copolymers is integrated with the diffuse motion of the nanoparticles.

A cell dynamical system (CDS), or cellular automaton, methodology is used to evolve the order parameter field for the microphase-separating copolymer melt [50,51]. The employment of CDS [rather than a conventional discretization

of Eq. (1)] significantly reduces the computational expense of the simulations. The discrete equations are of the form

$$\Psi(r, t+1) = G[\Psi(r, t)] - \langle G[\Psi(r, t)] - \Psi(r, t) \rangle - \Gamma(\Psi - f), \quad (6)$$

where a hyperbolic tangent model is included in the function G , although the results are insensitive to this choice of map [50]. In particular,

$$G[\Psi(r, t)] = A \tanh(\Psi) + \frac{\partial F_{cpl}}{\partial \Psi} + D[\langle \Psi(r, t) \rangle - \Psi(r, t)]. \quad (7)$$

In the current simulation, the parameters are assigned the following values: $A = 1.3$ and $D = 0.5$; these parameters correspond to an intermediate-to-strong segregation regime for the diblock. The operator $\langle * \rangle$ indicates the isotopic spatial average over the neighboring nodes, and $[\langle * \rangle - *]$ can be considered as a discrete generalization of the Laplacian. In three dimensions, the spatial average on a cubic lattice is given by

$$\langle * \rangle = \frac{6}{80} \sum_{NN} * + \frac{3}{80} \sum_{NNN} * + \frac{1}{80} \sum_{NNNN} *, \quad (8)$$

where NN, NNN, and NNNN represent the nearest, next-nearest, and next-next-nearest neighbors, respectively [52]. This form of spatial averaging operator ensures isotropy.

B. Determining the micromechanical behavior of solid polymeric composites

A lattice spring model enables the micromechanical investigation of a solid polymer to be undertaken. The model discretizes the continuum elastic behavior of a given material onto a simple cubic lattice. This lattice consists of a network of nearest and next-nearest neighbor interactions, which are harmonic in nature. These harmonic interactions (springs) result in linear forces between lattice sites (nodes), which enable the emergence of linear elastic behavior. The energy associated with a node m in the lattice is taken to be of the form

$$E_m = \frac{1}{2} \sum_n (\mathbf{u}_m - \mathbf{u}_n) \cdot \mathbf{M}_{mn} \cdot (\mathbf{u}_m - \mathbf{u}_n), \quad (9)$$

where the summation is over all the neighboring nodes, n , connected to m by a spring. The term \mathbf{u}_m is the displacement of node m from its original position, and \mathbf{M}_{mn} is a symmetric matrix that introduces the elastic properties of the springs, through central and noncentral force constants.

It has been shown that this system of springs obeys, to first order in the displacement, the equations of continuum elasticity theory for an isotropic medium, whose elastic constants can be determined in terms of the elements of the matrices \mathbf{M}_{mn} [39]. The Young's modulus E and Poisson's ratio ν are of the form

$$E = \frac{5k(2k+3c)}{4k+c}, \quad \nu = -\frac{k-c}{c+4k}, \quad (10)$$

where k and c are the central and noncentral force constants, respectively [39].

The force constants are initially associated with the nodes. Nodes are assigned different values depending upon the location in the material where they are situated. The force constants for the springs are then averaged from the nodes where they connect. The harmonic form of the energy results in forces that are linearly dependent upon the displacement of the nodes. If forces are applied to the boundary nodes, and the spring constants specified, then the nodal displacements can be obtained through a set of sparse linear equations. These equations are solved using a conjugate gradient method to find the equilibrium configuration that corresponds to no net force at each node [39].

In order to present relevant deformation fields, the stress and strain tensors are calculated from the forces and displacements. The strain tensor can be obtained through a finite difference approximation of the displacement field. A central difference approximation can be used,

$$\delta_x u_{(i,j,k)} = \frac{1}{12} [-u_{(i+2,j,k)} + 8u_{(i+1,j,k)} - 8u_{(i-1,j,k)} + u_{(i-2,j,k)}], \quad (11)$$

where $u_{(i,j,k)}$ is the displacement field at coordinates i, j, k , and h is the initial distance between adjacent nodes; alternatively, forward or backward approximations are considered at system boundaries. The stress tensor is directly obtainable from the forces acting on a node (the center of a cubic unit cell) [40],

$$\sigma_{ij} = \frac{\sum_m F_m \cdot n_{ij}^m}{A}. \quad (12)$$

Here, \sum_m represents a sum over the cube surfaces, F_m is the force on any surface m of the cubic cell, while n_{ij}^m is a unit vector either normal or parallel to the surface m , and A is the surface area. The scalar stress and strain values quoted here correspond to the normal stress and strain components in the tensile direction.

In order to assess the effective reinforcement provided by the particles within the composite, we determine the relative quantities $(u - u_0)/u_0$, where u is the strain field and u_0 is the homogeneous response of the unreinforced polymeric matrix. The average strain in the system can be determined through the average nodal displacements at the system boundaries, in the tensile direction. The average strain and the applied stress can then be used to calculate the Young's modulus (stress of a material divided by its strain). This allows the global stiffness of this locally heterogeneous material to be determined.

As noted above, the elastic properties of the springs within an LSM simulation are assigned values depending upon whether the node is situated within a particle or the

polymer matrix, as dictated by the results of the CH-BD calculation. In order to accurately capture the deformation fields in the vicinity of the particles within the LSM, the system size is doubled from that of the CH-BD simulation. An LSM consisting of 148^3 nodes is utilized; the central 128^3 nodes are assigned elastic properties as a function of the particle and polymer positions in the CH-BD calculation. The system is extended by ten unit lengths in all directions, taking values from the periodicity of the CH-BD simulation, therefore ensuring that all areas of the CH-BD model are represented by bulk nodes in the LSM simulation.

III. RESULTS

A. Uniform particle size

We initially consider the effects of diblock copolymer architecture and particle volume fraction on the resultant morphological and mechanical characteristics. In the following simulations, the parameters M and M_p [in Eqs. (1) and (5), respectively] are set equal to 1. Three different diblock copolymers are considered, corresponding to the following parameters: (a) $\Gamma = 0.004$ and $f = 0.0$, (b) $\Gamma = 0.016$ and $f = 0.0$, and (c) $\Gamma = 0.004$ and $f = 0.2$ [see Eq. (1)]. The parameter Γ is inversely proportional to N^2 , where N is the degree of polymerization of the copolymer. Thus, an increase in Γ corresponds to a decrease in the domain size. Varying f from 0.0 to 0.2 changes the composition from 50:50 to 60:40 (particles are incorporated into the minority phase). Therefore, the effects of domain size and composition are taken into consideration. A range of particle volume fractions, varying from 5% to 25%, are also considered, where the particle radius is three unit lengths (six unit lengths in the LSM). This range in volume fraction of particles corresponds to a variation in the number of particles from 116 to 580 in the simulations.

The morphology of a filled diblock copolymer system at late times ($t = 50\,000$) is presented in Fig. 1. The parameters of the diblock copolymer are $\Gamma = 0.004$ and $f = 0.0$, and the volume fraction of particles is 20%. The isosurface of the diblock copolymer at an order parameter of zero (midway between phase A and phase B) is colored blue, while the regions where a positive order parameter intersects the system boundaries (termed isocaps) are colored red. In other words, the red regions mark the B phase and the transparent regions indicate the A phase. The particles are colored black, and are clearly confined within the transparent A phase of the diblock. The system shows elements of lamellar ordering on a short scale, however, the lamellas are interconnected, and the overall morphology is closer to a bicontinuous structure. While the system will tend towards the thermodynamic limit of a perfect lamellar phase, the time scales for reaching this state through a dynamic model are prohibitively large. In experimental systems, similar morphologies are found because again it takes long times to reach perfectly ordered phases and the system can get kinetically trapped.

In order to quantify the confinement of nanoparticles within the diblock copolymer domains, the particle correlation function is presented in Fig. 2. The particle correlation function adopted in this study is defined as $g(r)$

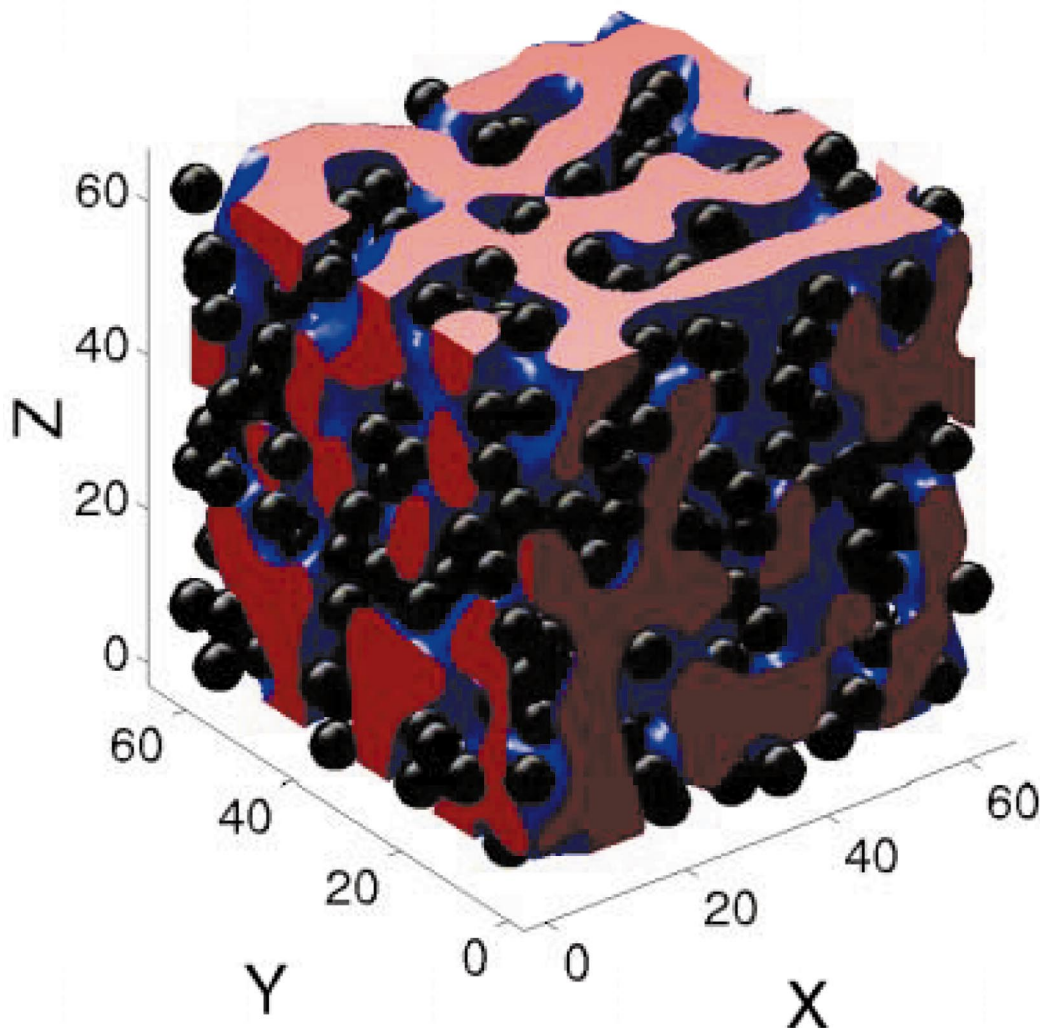


FIG. 1. (Color) Three-dimensional morphology of a filled diblock copolymeric system. An isosurface inbetween the A and B components is colored blue, isocaps are colored red, and the particles are colored black.

$= V \langle \sum_i \sum_{j \neq i} \delta(r - r_{ij}) \rangle / (4\pi r^2 N_p^2)$, where V is the volume of the system and N_p is the number of particles. The results are averaged over three independent runs. For clarity, only two diblock copolymer systems are shown ($\Gamma = 0.004$ and Γ

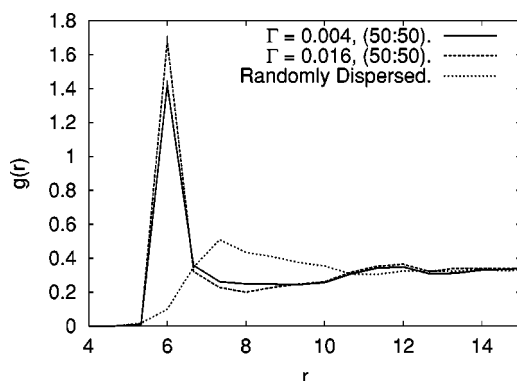


FIG. 2. The pair correlation function [defined as $g(r) = V \langle \sum_i \sum_{j \neq i} \delta(r - r_{ij}) \rangle / (4\pi r^2 N_p^2)$] for particles confined in two diblock copolymer systems and for randomly dispersed particles.

$= 0.016$ at $f=0.0$) as the third exhibited similar results. There is only one discernible peak at a distance of six unit lengths, which corresponds to the diameter of the particles. This reveals that the system of particles exhibit strong short range order, but do not display long range order. The particles are forced to lie within close proximity of each other due to the confinement within the diblock copolymer, but long range order is suppressed due to the tortuous structure of the diblock domains. For comparison, the particle correlation functions for an equivalent number of randomly dispersed particles, which exhibit no such confinement, are also presented. As can be seen, there is no local ordering of the particle positions and the peaks observed in the diblock copolymer systems are no longer present.

To assess the consequences of such morphological variations upon the resultant mechanical properties of the macroscopic material, we now use the output from our hybrid CH and Langevin dynamics simulations as the input for the LSM. The elastic deformation of the structures is undertaken, with both the force constants of the A and B phases being set to unity, while the particles are assigned a force constant of

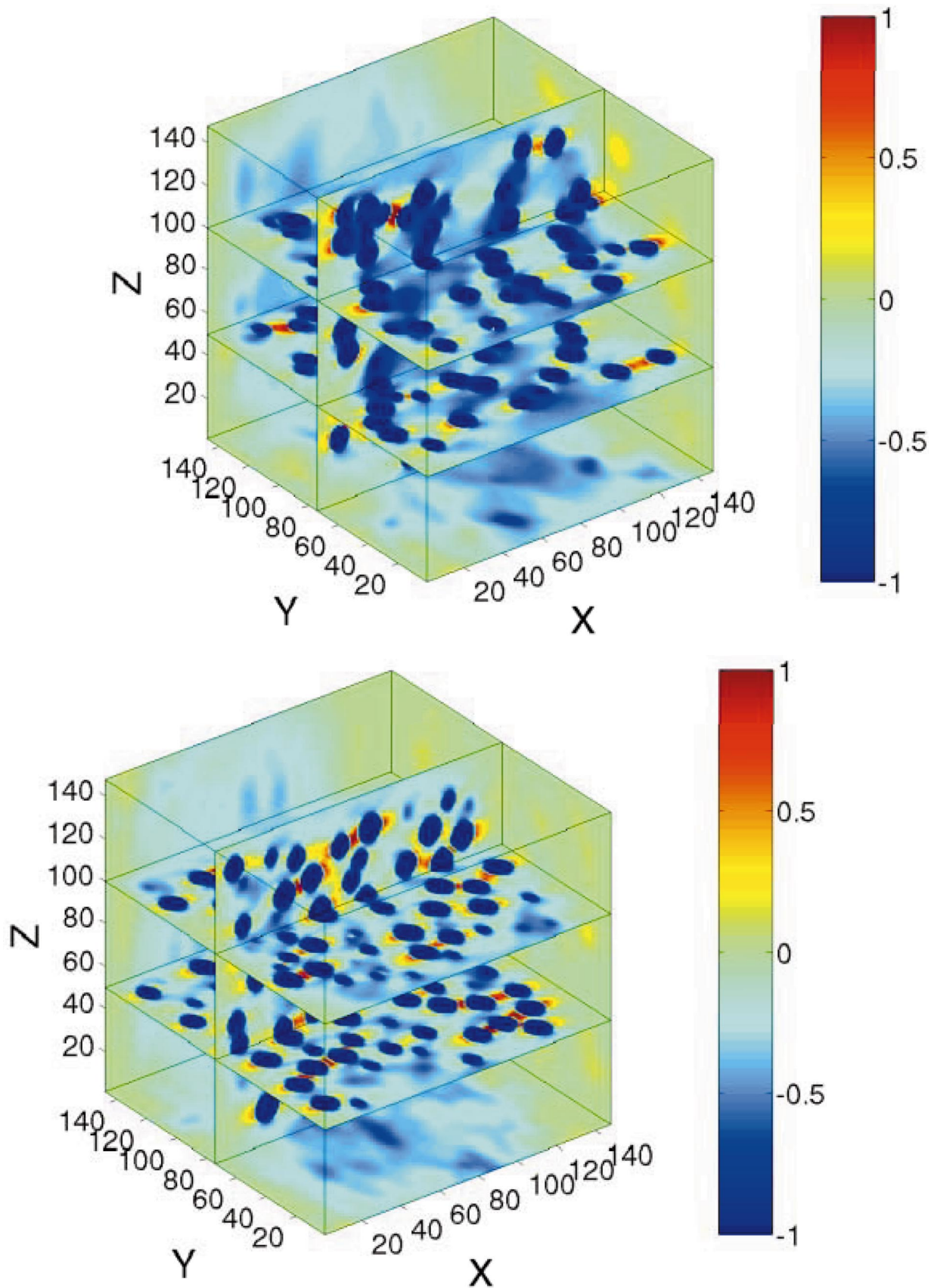


FIG. 3. (Color) The relative strain fields [defined as $(u - u_0)/u_0$, where u_0 is the response of the unreinforced polymeric matrix] for (a) a system where the particles are confined within the domains of a diblock copolymer and (b) a system consisting of randomly dispersed particles.

100. Thus, the effects of particle distribution are of primary interest in the current investigations, and the parameters are consistent with experimental values for filled polymers [53].

The local relative strain field, as a result of the application of a constant stress at the simulation boundaries, for a system where the particles are confined within the domains of a diblock copolymer ($\Gamma = 0.004$ and $f = 0.0$) is depicted in Fig. 3(a). The corresponding relative strain field for a system consisting of randomly dispersed particles is presented in Fig. 3(b). The three-dimensional strain fields are displayed as orthogonal contours through the simulation. In both systems, the volume fraction of particles is 20%. The particles are clearly apparent as the dark blue regions of low strain. In particular, the strain values within the particles are significantly lower than that of the matrix, due to the large disparity in elastic constants. The inability of stiff particles to deform to the same extent as the neighboring matrix results in strain concentrations at the particle-matrix interface. These strain concentrations lie along the tensile direction and emanate from the center of a particle. Perpendicular to the tensile direction, the lower deformations within the particle inhibit the deformation of the matrix and result in lower strain fields.

It is apparent from Fig. 3(a) that the diblock-confined particles are clustered together, while the particles in Fig. 3(b) are more randomly dispersed. It is this clustering of the confined particles that is of primary interest. In order to characterize the particle clusters, and determine whether or not geometric percolation occurs, we define particles that are closer than a certain distance to be part of the same cluster. Here, we adopt a unit length in the LSM simulations as this characteristic distance. Using this definition, we find that the confined particle system in Fig. 3(a) forms a percolating cluster. (We note that Ginzburg *et al.* [23] found the percolation threshold for particles confined in a similar diblock matrix to be $\approx 10\%$.)

The percolating structure inhibits the deformation of the entire material and results in significant reductions in the strain fields, as can be seen by the presence of the purple domains in Fig. 3(a). Alternatively, the randomly dispersed

system shows isolated regions of strain relaxation within the particles, but the inhibition of the neighboring matrix is less dramatic than in Fig. 3(a). Consequently, the strain concentrations (shown in red and yellow) within the matrix of the randomly dispersed system are also more pronounced as regions within the matrix attempt to deform to the same extent as domains that neighbor the scattered particles. Such areas of strain concentration are less apparent in Fig. 3(a). These plots indicate that the confinement of nanoparticles within one of the domains of the bicontinuous structure leads to a continuous network of stiff material, which reduces the overall strain field within the system.

In order to quantify the deformation of the above confined and randomly dispersed particle systems, the cumulative distribution functions of the local strain fields are plotted in Fig. 4. The cumulative distribution function is defined as the probability that the field in the system takes a value less than or equal to a specific amount. A comparison between confined and randomly dispersed particle systems is made for particle volume fractions varying from 5% to 25%. The lower strains are invariably associated with the stiffer particles, while the regions of higher strains correspond to the matrix. At 5%, there would appear to be little difference between the two systems, since the confined particles do not percolate at such a low value. At higher particle volume fractions, the disparity between the two systems becomes more apparent, with the confined particle systems possessing significantly lower strain fields. As noted above, the geometric percolation inhibits the local strain fields, and therefore stiffens the composite material.

In Fig. 5, we plot the percentage increase in the Young's modulus relative to the unreinforced polymer for the various systems described above. This parameter is a measure of the macroscopic mechanical properties of these composites. The results are averaged over three independent runs, with the error bars indicating the standard deviation. The three cases involving particles confined within the domains of diblock copolymers are significantly stiffer than the system containing randomly dispersed particles. There is no clear difference between the three confined particle systems, with the error bars showing a clear overlap. For the systems studied here, it is not possible to distinguish effects that diblock copolymer architecture or composition may have on the reinforcement efficiency of the nanoparticle fillers. There is, however, a significant benefit in confining the particles within the diblock copolymer domains.

B. Binary particle systems

We also investigate the effects of adding a binary particle mixture to the copolymer matrix. The particles in the binary mixture are chemically identical (i.e., they both favor the A phase), but differ in size. The smaller particles have a radius of 2 and the larger particles have a radius of three unit lengths. These studies provide insight into the role that polydispersity in particle size plays in the mechanical properties of the composite. The total volume fraction of particles is held fixed at 20% and the ratio of small to large fillers is varied between the limiting cases of all small (1564 par-

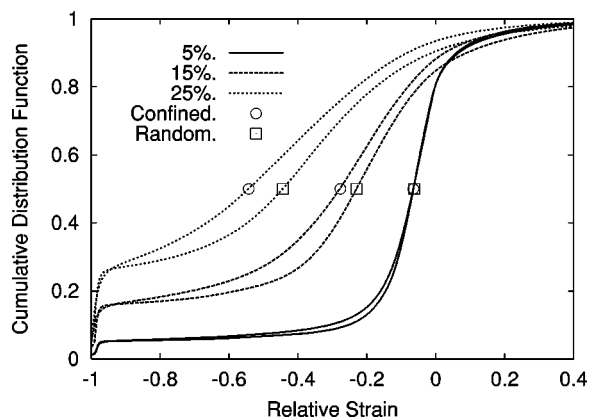


FIG. 4. The cumulative distribution function of the relative local strain field for systems consisting of randomly dispersed particles and systems where the particles are confined within the domains of a diblock copolymer.

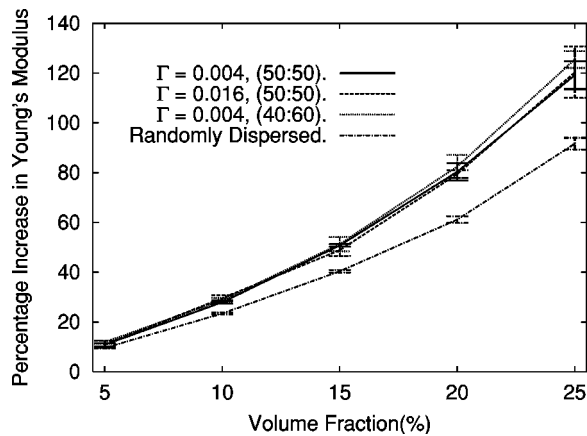


FIG. 5. The percentage increase in Young's modulus as a function of particle volume fraction. Systems containing particles confined within the domains of various diblock copolymers are compared with a system consisting of randomly dispersed particles.

ticles) and all large (464 particles). A comparison of the results for the purely large and small fillers yields insight into the effects of particle size on the behavior of the system. In these studies, the parameters that characterize the diblock copolymers are fixed at $\Gamma = 0.004$ and $f = 0.0$.

Figure 6 shows the morphology for a system containing 10% of large and 10% of small particles. The particles are again clearly confined within the *A* domains of the diblock copolymer. Note that the particles selectively swell these compatible *A* regions, giving the diblock matrix in Fig. 6 an asymmetric appearance. However, here as in the other cases described in this section, the copolymer is a symmetric diblock.

It is also clear from Fig. 6 that the small particles can readily penetrate and localize in regions between the large particles. At a fixed particle volume fraction, decreasing the size of the particles results in an increase in the total *number* of particles and hence, an effective increase in the particulate surface area. Consequently, there is a greater surface area available for possible polymer-particle interactions. To illustrate this point, we define V_p as the volume fraction of poly-

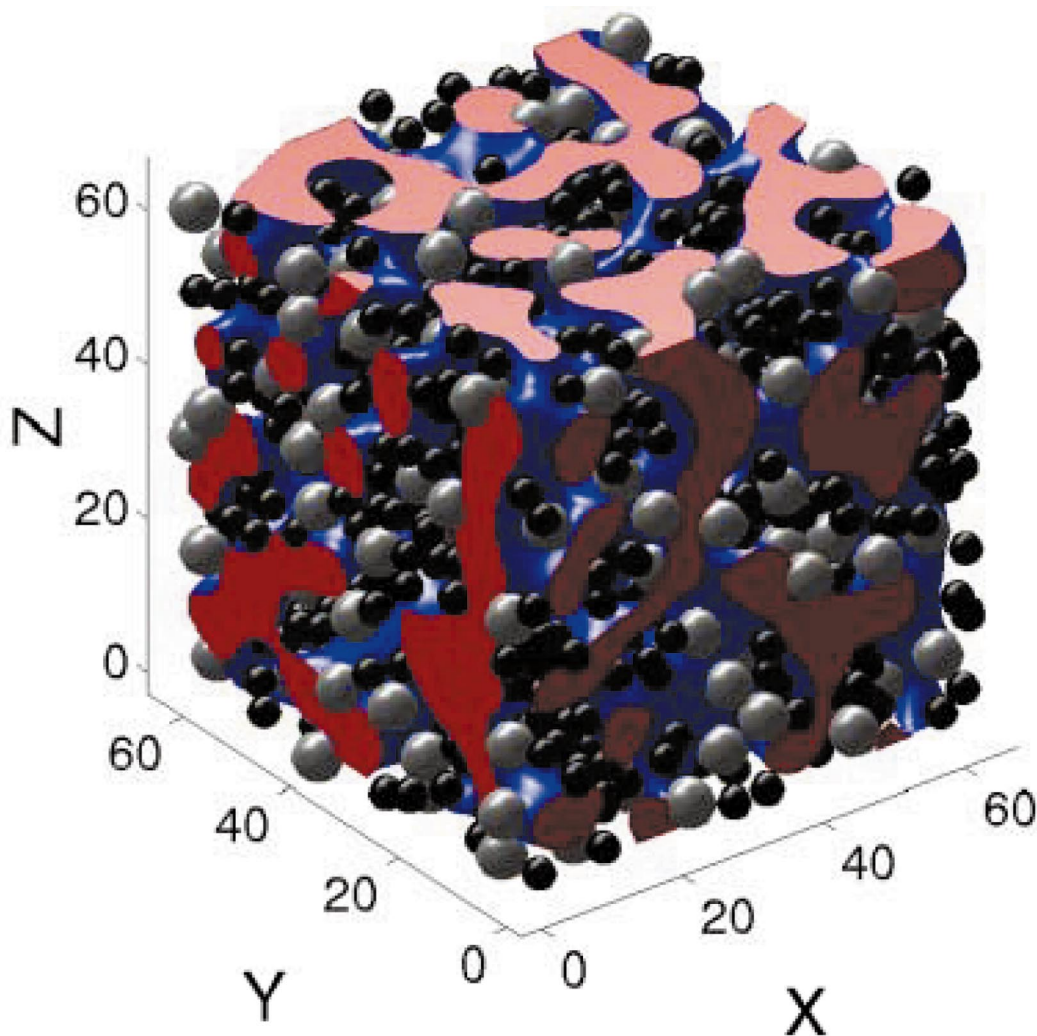


FIG. 6. (Color) Three-dimensional morphology of a filled diblock copolymeric system. An isosurface in between the *A* and *B* components is colored blue, isocaps are colored red, and the small and large particles are colored black and gray, respectively.

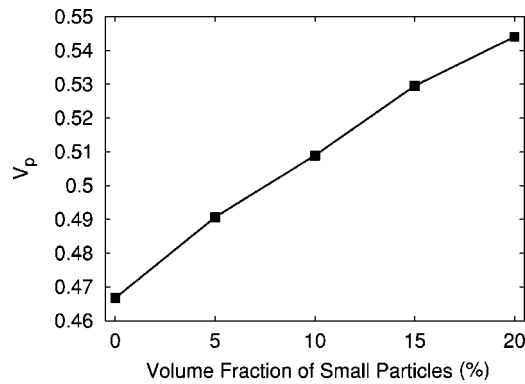


FIG. 7. The volume fraction of polymeric material that is within a given distance (a unit length) of any particles, V_p , as a function of the volume fraction of small particles.

meric material (A and B) that is within a given distance (a unit length) of any particles and plot V_p as a function of the volume fraction of small particles (see Fig. 7). The results are averaged over three runs and the standard deviations were found to be negligible. As the volume fraction of small particles is increased, the particles come in contact with and affect a greater volume of the matrix.

The fraction of particles that are a part of the largest cluster, P , is plotted as a function of the volume fraction of small particles in Fig. 8. The data are averaged over three runs, with the error bars corresponding with the standard deviation. Geometric percolation occurred in all systems. Since at a fixed volume fraction, there are a greater number of small particles than large ones, these fillers would be expected to cluster to a greater extent than the larger species (as the characteristic distance used to indicate clustering is not radius dependent, but is fixed at one unit in our studies). This is in fact the case, with the fraction of particles in the main cluster approaching one with increasing number of small particles. Even though small particles are more dispersed (as indicated by Fig. 7), they still cluster to a greater degree within the domain structure of the diblock copolymer (in part, because there are a greater number of them than large particles). This increase in clustering is expected to translate through to the mechanical properties.

Figure 9 reveals the relative strain field for a system containing 10% large particles and 10% small particles. The regions of low strain, corresponding to the stiffer particles, are clearly observed as before. Now, however, the clustering of particles is more apparent than that in Fig. 3(a). A significant difference between the cases in Figs. 3(a) and 9 is the area over which these particles cluster. The smaller particles spread out over a greater volume of the material and inhibit the deformation of the matrix to a greater degree than in the system containing just large particles. Effectively, a larger volume of polymer matrix is trapped or surrounded by the particles and therefore less capable of deforming.

Quantitatively, the effects of particle size can be seen in Fig. 10, which depicts the cumulative distribution function of the local relative strain as the volume fraction of particles varies from being 20% large to 20% small. The data are averaged over three independent runs. The plots show that

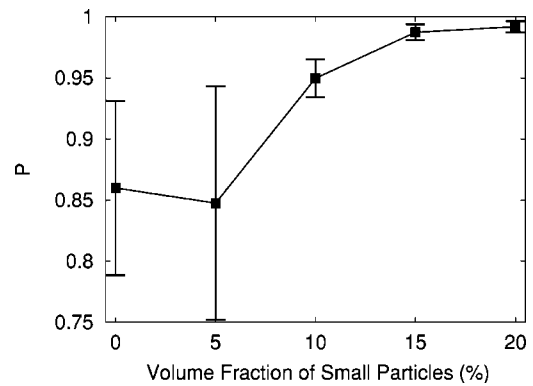


FIG. 8. The fraction of particles that are a part of the largest cluster as a function of the volume fraction of small particles. The overall volume fraction of small and large particles is maintained at 20%.

20% of the system possesses lower strains due to the 20% of stiff particles present within the composite; however, in the upper 80% of the system, a gradual trend is observed. The deformations in the matrix are increasingly inhibited as the volume fraction of smaller particles is increased.

The lower strain fields due to the decrease in particle size have a direct impact on the Young's modulus of the macroscopic material. The percentage increase in Young's modulus is plotted in Fig. 11, as a function of the volume fraction of small particles. The data are averaged over three runs, were the error bars represent the standard deviations. An increase in Young's modulus of over 30% is observed as the particle size is altered from all large to all small. This is attributable to an increase in the total particle surface area, a greater degree of clustering, and an increase in the volume of polymeric material that is effectively trapped by the particles. These effects result in lower strains throughout the system and, hence, an increase in the global Young's modulus.

IV. CONCLUSIONS

Through a combination of numerical techniques, we were able to interrelate the structure and micromechanical behavior of the copolymer-nanoparticle composites. Through the CH-BD calculations, we could determine the effects of the microphase separation of the diblocks on the spatial distribution of the mobile particles. Through the LSM, we could capture the elastic deformation of the resultant hybrid material. Furthermore, we could investigate the behavior of systems that contain up to 1564 particles. For randomly dispersed fillers, simulations involving a relatively low number of particles can be sufficient to describe the overall stiffness of the material and thus, can be large enough to encompass a representative volume element (RVE) of the composite. However, the tortuous spatial arrangement of particles confined in diblock copolymers introduces an additional length scale, that of the domain size. To determine the mechanical behavior of such complex materials, it is important to consider the morphology of a sufficiently large system that captures both the unique structural characteristics of the copolymer domains and the particles' spatial arrangement, which is, in part, templated by these diblock domains. The LSM has

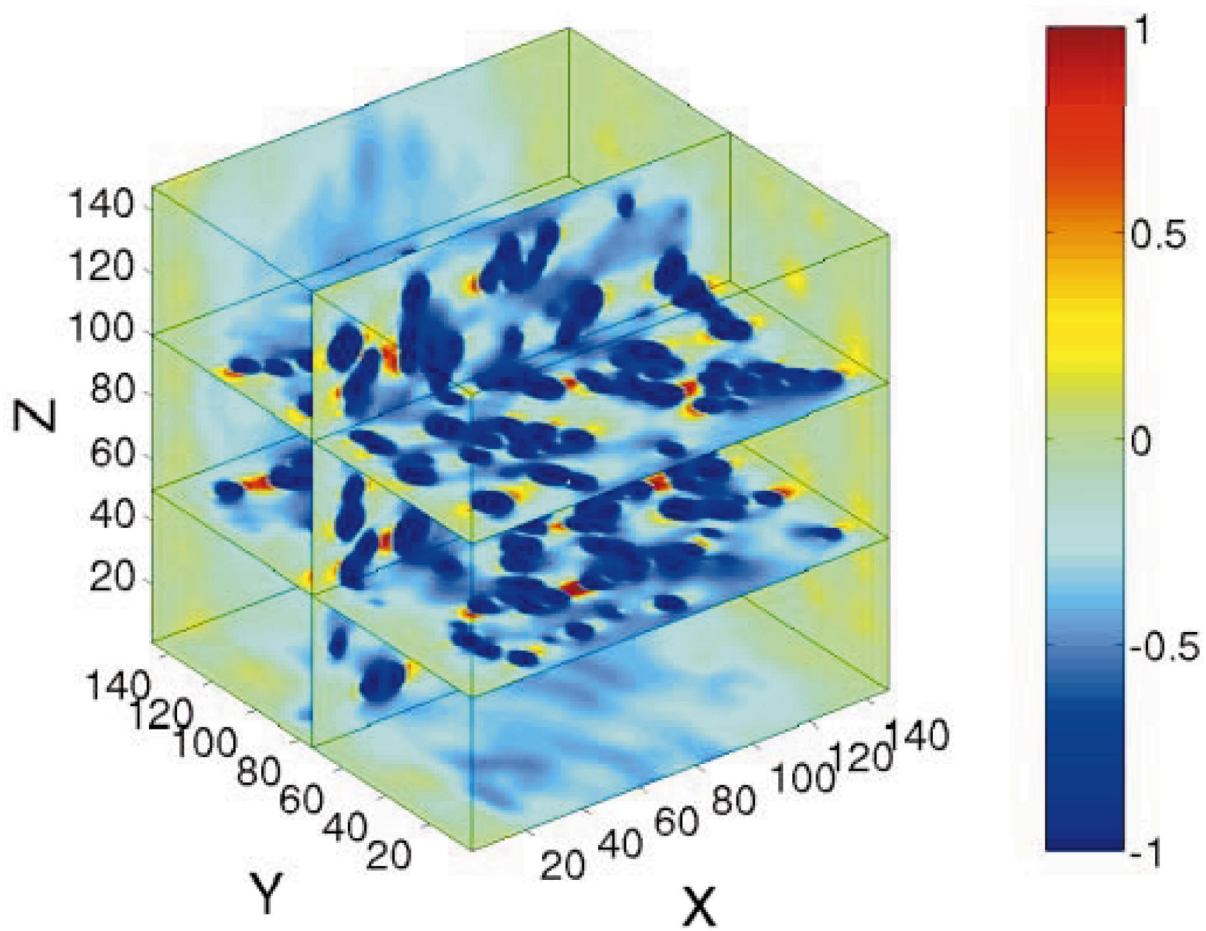


FIG. 9. (Color) The relative strain fields [defined as $(u - u_0)/u_0$, where u_0 is the response of the unreinforced polymeric matrix] for a system containing a 10% volume fraction of small and a 10% volume fraction of large particles, confined within the domains of a diblock copolymer.

proven to be ideally suited for simulating the micromechanics of such large systems. While the utility of the LSM in analyzing two-dimensional RVEs has recently been reported [54], it would appear that this technique might also prove

useful in similar three-dimensional analyses.

Through the selective incorporation of nanoparticles into the domains of a diblock copolymer, three-dimensional bi-continuous nanoparticle structures were formed. As the volume fraction of particles was increased, geometric percola-

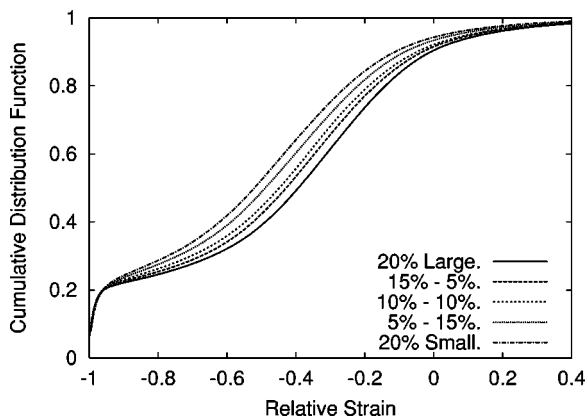


FIG. 10. The cumulative distribution function of the relative local strain field for systems containing various volume fractions of small and large particles; varying from 20% large to 20% small. The overall volume fraction of small and large particles is maintained at 20%.

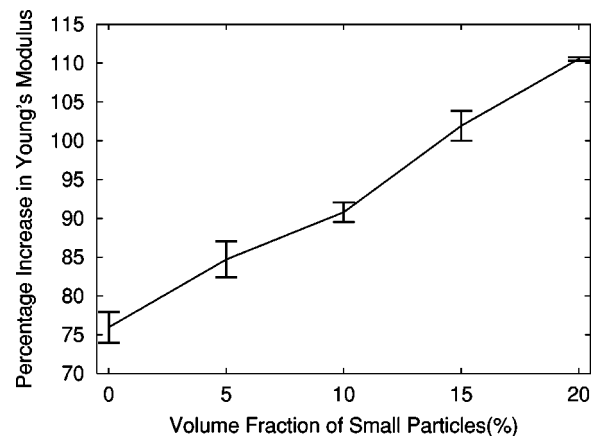


FIG. 11. The percentage increase in Young's modulus as a function of small particle volume fraction. The overall volume fraction of small and large particles is maintained at 20%.

tion of the particles occurred, and the particles effectively formed a rigid network throughout the system. The deformations within the polymer matrix are significantly suppressed by the presence of this rigid nanostructural network, and the global stiffness of the material is notably increased. It is worth noting that for materials containing randomly dispersed spheres, rods and platelets, the rods and platelets offer superior reinforcement over the spheres [46]. Therefore, the mechanical properties of diblock copolymers filled with such high aspect ratio particles may prove to be of particular interest.

Varying the size of the monodisperse particles and introducing bidispersity in the particle size were shown to exert an appreciable influence over both the morphology of the diblock copolymer and the resultant mechanical properties of the solid material. Systems containing small fillers exhibited a greater degree of clustering between the particles. This

behavior could explain the increased stiffness that was observed in the corresponding macroscopic material. Also of considerable consequence is the volume of polymeric material that is effectively trapped between neighboring nanoparticles. For a fixed volume fraction of particles, as the particle size is decreased, the number of particles increases. Consequently, the volume of material in which the particles are dispersed increases, and the deformation of a greater volume of interparticle polymeric material is inhibited.

We conclude that the inclusion of nanoparticles into a bicontinuous diblock copolymer structure results in a significant increase in the reinforcement efficiency of the fillers. As polymeric nanocomposites become increasingly important, such confinement effects will play a dominant role in optimizing their mechanical behavior, and result in an expansion of potential applications to which such materials could be employed.

-
- [1] P.P. Soo, B.Y. Huang, Y.I. Jang, Y.M. Chiang, D.R. Sadoway, and A.M. Mayes, *J. Electrochem. Soc.* **146**, 32 (1999).
- [2] N. Hasegawa, H. Okamoto, M. Kawasumi, and A. Usuki, *J. Appl. Polym. Sci.* **74**, 3359 (1999).
- [3] T.L. Morkved, P. Wiltzius, H.M. Jaeger, D.G. Grier, and T.A. Witten, *Appl. Phys. Lett.* **64**, 422 (1994).
- [4] B.H. Lin, T.L. Morkved, H.M. Jaeger, D.G. Grier, and T.A. Witten, *J. Appl. Phys.* **85**, 3180 (1999).
- [5] R.W. Zhener, W.A. Lopes, T.L. Morkved, H. Jaeger, and L.R. Sita, *Langmuir* **14**, 241 (1998).
- [6] Y. Fink, A.M. Urbas, M.G. Bawendi, J.D. Joannopoulos, and E.L. Thomas, *J. Lightwave Technol.* **LT17**, 1963 (1999).
- [7] D.H. Cole, K.R. Shull, P. Baldo, and L. Rehn, *Macromolecules* **32**, 771 (1999).
- [8] B. Hamdoun, D. Ausserre, S. Joly, Y. Gallot, V. Cabuil, and C. Clinard, *J. Phys. II* **6**, 493 (1996); **6**, 503 (1996); **6**, 1207 (1996).
- [9] V. Lauter-Pasyuk, H.J. Lauter, D. Ausserre, Y. Gallot, V. Cabuil, B. Hamdoun, and E.I. Kornilov, *Physica B* **1092**, 241 (1998).
- [10] J. Huh, V. Ginzburg, and A.C. Balazs, *Macromolecules* **33**, 8085 (2000).
- [11] G.J.A. Sevink, A.V. Zvelindovsky, B.A.C. van Vlimmeren, N.M. Maurits, and J.G.E.M. Fraaije, *J. Chem. Phys.* **110**, 2250 (1999).
- [12] R. Thompson, V. Ginzburg, M. Matsen, and A.C. Balazs, *Macromolecules* **35**, 1060 (2002).
- [13] E. Jeung, T.H. Galow, J. Schotter, M. Bal, A. Ursache, M.T. Tuominen, C.M. Stafford, T.P. Russell, and V.M. Rotello, *Langmuir* **17**, 6396 (2001).
- [14] W.A. Lopes and H.M. Jaeger, *Nature (London)* **414**, 735 (2001).
- [15] J. Groenewold and G. Fredrickson, *Eur. Phys. J. E* **5**, 171 (2001).
- [16] J.X. Ren, A.S. Silva, and R. Krishnamoorti, *Macromolecules* **33**, 3739 (2000).
- [17] Y.H. Ha and E.L. Thomas, *Macromolecules* **35**, 4419 (2002), and references therein.
- [18] V.V. Ginzburg, F. Qiu, M. Paniconi, G. Peng, D. Jasnow, and A.C. Balazs, *Phys. Rev. Lett.* **82**, 4026 (1999).
- [19] V.V. Ginzburg, G. Peng, F. Qiu, D. Jasnow, and A.C. Balazs, *Phys. Rev. E* **60**, 4352 (1999).
- [20] G. Peng, F. Qiu, V.V. Ginzburg, D. Jasnow, and A.C. Balazs, *Science* **288**, 1802 (2000).
- [21] A.C. Balazs, V.V. Ginzburg, F. Qiu, G. Peng, and D. Jasnow, *J. Phys. Chem. B* **104**, 3411 (2000).
- [22] V.V. Ginzburg, C. Gibbons, F. Qiu, G. Peng, and A.C. Balazs, *Macromolecules* **33**, 6140 (2000).
- [23] V.V. Ginzburg, F. Qiu, and A.C. Balazs, *Polymer* **43**, 461 (2002).
- [24] G.A. Buxton and A.C. Balazs, *Interface Sci.* **11**, 175 (2003).
- [25] D.E. Fogg, L.H. Radzilowski, R. Blanski, R.R. Schrock, and E.L. Thomas, *Macromolecules* **30**, 417 (1997).
- [26] R.W. Zhener, W.A. Lopes, T.L. Morkved, H. Jaeger, and L.R. Sita, *Langmuir* **14**, 241 (1998).
- [27] K. Tsutsumi, Y. Funaki, Y. Hirokawa, and T. Hashimoto, *Langmuir* **15**, 5200 (1999).
- [28] T. Christman, A. Needleman, and S. Suresh, *Acta Metall.* **37**, 3029 (1989).
- [29] J. Llorca, A. Needleman, and S. Suresh, *Acta Metall. Mater.* **39**, 2317 (1991).
- [30] C.L. Hom and R.M. McMeeking, *Int. J. Plast.* **7**, 255 (1991).
- [31] D.F. Watt, X.Q. Xu, and D.J. Lloyd, *Acta Mater.* **44**, 789 (1996).
- [32] C.I.A. Thomson, M.J. Worswick, A.K. Pilkey, D.J. Lloyd, and G. Burger, *J. Mech. Phys. Solids* **47**, 1 (1999).
- [33] A. Needleman, *J. Appl. Mech.* **54**, 525 (1987).
- [34] A.A. Gusev, *J. Mech. Phys. Solids* **45**, 1449 (1997).
- [35] H.J. Böhm and W. Han, *Modell. Simul. Mater. Sci. Eng.* **9**, 47 (2001).
- [36] M. Born and K. Huang, *Dynamical Theory of Crystal Lattices* (Oxford University Press, Oxford, 1954).
- [37] G.N. Hassold and D.J. Srolovitz, *Phys. Rev. B* **39**, 9273 (1989).
- [38] P.N. Sen and M.F. Thorpe, *Phys. Rev. B* **15**, 4030 (1977).
- [39] G.A. Buxton, C.M. Care, and D.J. Cleaver, *Modell. Simul.*

- Mater. Sci. Eng. **9**, 482 (2001).
- [40] L. Monette and M.P. Anderson, *Modell. Simul. Mater. Sci. Eng.* **2**, 53 (1994).
- [41] K.A. Snyder, E.J. Garoczi, and A.R. Day, *J. Appl. Phys.* **72**, 5948 (1992).
- [42] L. Monette and M.P. Anderson, *Semicond. Semimetals* **28**, 1095 (1993).
- [43] L. Monette, M.P. Anderson, and G.S. Grest, *J. Appl. Phys.* **75**, 1155 (1994).
- [44] M. Ostoja-Starzewski, P.Y. Sheng, and I. Jasiuk, *Eng. Fract. Mech.* **58**, 581 (1997).
- [45] K. Alzebdeh, A. Al-Ostaz, I. Jasiuk, and M. Ostoja-Starzewski, *Int. J. Solids Struct.* **35**, 2537 (1998).
- [46] G.A. Buxton and A.C. Balazs, *J. Chem. Phys.* **117**, 7649 (2002).
- [47] J.W. Cahn and J.E. Hilliard, *J. Chem. Phys.* **28**, 258 (1958).
- [48] J.W. Cahn, *J. Chem. Phys.* **42**, 93 (1965).
- [49] Y. Oono and M. Bahiana, *Phys. Rev. Lett.* **61**, 1109 (1988).
- [50] Y. Oono and S. Puri, *Phys. Rev. Lett.* **58**, 836 (1987).
- [51] Y. Oono and S. Puri, *Phys. Rev. A* **38**, 434 (1988).
- [52] A. Shinozaki and Y. Oono, *Phys. Rev. E* **48**, 2622 (1993).
- [53] N.G. McCrum, C.P. Buckley, and C.B. Bucknall, *Principles of Polymer Engineering* (Oxford University Press, Oxford, 1997).
- [54] M. Jiang, K. Alzebdeh, I. Jasiuk, and M. Ostoja-Starzewski, *Acta Mech.* **148**, 63 (2001).